Total-scattering descriptions of local and cooperative distortions in the oxide spinel $Mg_{1-x}Cu_xCr_2O_4$ with dilute Jahn-Teller ions

Daniel P. Shoemaker* and Ram Seshadri†
Materials Department and Materials Research Laboratory, University of California, Santa Barbara, California 93106, USA
(Received 27 September 2010; published 10 December 2010)

The normal spinel oxide $MgCr_2O_4$ is cubic at room temperature while the normal spinel $CuCr_2O_4$ is tetragonal as a consequence of the Jahn-Teller activity of Cu^{2+} on the tetrahedral sites. Despite different end-member structures, a complete solid solution of $Mg_{1-x}Cu_xCr_2O_4$ can be prepared with compounds of composition $x=0.43$ displaying a first-order phase transition at room temperature. Reverse Monte Carlo analysis of total neutron scattering on data acquired between 300 and 15 K on samples with $x=0.10$, 0.20, and 0.43 provides unbiased local and average structure descriptions of the samples, including an understanding of the transition from local Jahn-Teller distortions in the cubic phase to cooperative distortions that result in a tetragonal structure. Distributions of continuous symmetry measures help to understand and distinguish distorted and undistorted coordination around the tetrahedral site in the solid solutions. Magnetic exchange bias is observed in field-cooled hysteresis loops of samples with dilute Cu^{2+} concentration and in samples with tetragonal-cubic phase coexistence around 300 K.

DOI: 10.1103/PhysRevB.82.214107 PACS number(s): 71.70.Ej, 61.05.fm, 75.50.Tt

I. INTRODUCTION

The propensity of octahedral Cu^{2+} ions in oxide structures to display Jahn-Teller (JT) distortions is intimately linked to magnetism and superconductivity in systems derived from La_2CuO_4.[1,2] While less common, tetrahedral Cu^{2+} on the A site of oxide spinels can also display JT activity. This distortion lowers symmetry by compressing the tetrahedron and thereby breaking the degeneracy of the partially occupied t_2 energy levels.[3,4] The crystal-field splittings of the ideal and distorted tetrahedra are shown schematically in Fig. 1.

Jahn-Teller distortions themselves are an intriguing theme in functional materials because they enable interplay between electronic and structural degrees of freedom. They have been most widely studied in the manganites, often derivatives of perovskite $LaMnO_3$.[5–7] In these compounds, Mn^{3+} has four $3d$ electrons with a singly occupied pair of e_g states in an octahedral crystal field. It is well established that elongation of the octahedron breaks the degeneracy and lowers the energy of the system.[8,9] The percolative nature of orbital ordering arising from cooperative JT distortion is believed to play a central role in colossal magnetoresistive behavior.[10]

In spinels, collective JT distortions on the A or B sites result in a reduction in symmetry from cubic $Fd\bar{3}m$ to tetragonal $I4_1/amd$ upon orbital ordering at the Jahn-Teller transition temperature T_{JT}. When only a fraction of occupied sites are JT active, cation clustering can lead to endotaxial coexistence of tetragonal (distorted) and cubic phases,[11–13] with strain-driven checkerboard patterns first studied in phase-separated CoPt alloys.[14–16] These Mn^{3+}-driven JT distortions are a product of unpaired $3d$ electrons, so self-assembled nanostructured magnetic films are under development.[17]

Few studies have examined the precise JT tendency of Cu^{2+} on the spinel A site. The effect of Cu^{2+} occupancy on T_{JT} and the electronic or magnetic properties remains sparsely investigated.[18–20] We expect there should be key differences between JT activity on the A and B sites of spinel. While BO_6 octahedra are edge sharing and form a pyrochlore sublattice, the AO_4 tetrahedra are isolated from each other in a diamond sublattice. The increased distance between A cations should hinder their cooperative behavior.

In this work, the structural effects of Cu^{2+} concentration x in the spinel solid solution $Mg_{1-x}Cu_xCr_2O_4$ are investigated by real- and reciprocal-space structural probes utilizing total neutron scattering. Discrepancies between the average and local structural are of particular interest. Specifically, we probe whether the coordination of JT-active Cu^{2+} and JT-inactive Mg^{2+} differ. Traditional Bragg diffraction analysis fails to resolve these differences because atoms on the same crystallographic site (here Cu and Mg on the spinel A site) are required to have identical surroundings. Electron paramagnetic resonance[21] and x-ray absorption[22] offer a confirmation that dilute Jahn-Teller cations create local distortions but these spectroscopic techniques do not yield any detailed structural information. We utilize the pair distribution function (PDF) because it provides a real-space description of the structure with distinct Cu-O and Mg-O distances.

Our previous PDF study of the spinel $CuMn_2O_4$ encountered many of the complications that make $Mg_{1-x}Cu_xCr_2O_4$ a difficult crystal structure to describe.[23] In that study, Cu and Mn are present with mixed valence on both A and B posi-

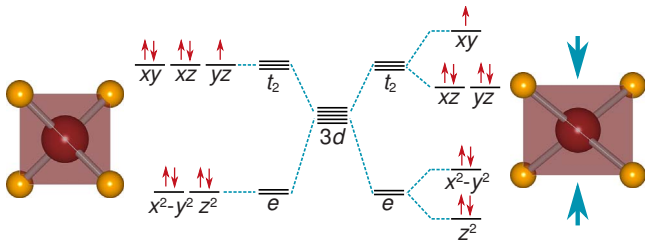

FIG. 1. (Color online) Crystal-field splitting of Cu^{2+} with a $3d^9$ electron configuration in an ideal tetrahedron (left) results in degeneracy in the t_2 orbitals. Jahn-Teller compression of the tetrahedron lifts the degeneracy (right) and results in a singly occupied xy orbital.

tions, and the surrounding oxygen polyhedra are cation dependent. We found that CuO_4 tetrahedra are significantly more distorted (as judged by bond angles) than MnO_4 tetrahedra and Cu avoids the tendency for JT distortion by disproportionating to Cu^+/Cu^{3+}. The situation for $Mg_{1-x}Cu_xCr_2O_4$ should be less complex: no valence mixing is present and Cu/Mg substitution is confined to the A site. The effect of central cation on MO_4 distortion is more isolated.

We employ large box modeling via reverse Monte Carlo (RMC) simulations as method of retrieving possible signatures of cation-dependent coordination from the PDF.[24,25] Supercells with thousands of atoms can be routinely simulated with modest computational requirements and the large sample size provides element-specific information due to the presence of many discrete atoms of each type. A crucial aspect of RMC simulations is determining straightforward metrics that describe how local crystalline structure differs from the average. The tendency for distortion of individual polyhedra has been characterized by analyzing bond lengths,[23] bond angles,[23,26,27] and geometric analysis.[28,29]

In this study, tetrahedral JT distortion is gauged using continuous symmetry measures (CSMs).[30,31] The particular strength of the CSM method is its ability to compare the symmetry of imperfect polyhedra, regardless of their size or orientation in space.[32,33] Extraction of CSM information from RMC simulation was recently performed as a test of structural rigidity in $Bi_2Ti_2O_7$ (Ref. 34) and is employed here to compare the symmetry of CuO_4, MgO_4, and AA_4 tetrahedra, thereby describing the preference for JT activity as a function of x and temperature.

II. METHODS

Powders of $Mg_{1-x}Cu_xCr_2O_4$ compounds were prepared by dissolving stoichiometric amounts of $Cu(NO_3)_2 \cdot 2.5H_2O$, $Mg(NO_3)_2 \cdot 6H_2O$, and $Cr(NO_3)_3 \cdot 9H_2O$ in water, followed by boiling to evaporate the solvent until a brown mass was formed, which was then ground and calcined in air at between 700 or 1000 °C for 10 h, then cooled at 10 °C/min. Laboratory x-ray diffraction (XRD) patterns were acquired using Cu $K\alpha$ radiation on a Philips X'Pert diffractometer at room temperature and a Bruker D8 diffractometer with an Anton Parr high-temperature stage. Magnetic properties were measured using a Quantum Design MPMS 5XL superconducting quantum interference device magnetometer. Time-of-flight (TOF) neutron scattering was performed on the NPDF instrument at Los Alamos National Laboratory. Rietveld refinements were performed using the XND code[35] for x-ray data and the GSAS-EXPGUI suite[36] for the TOF data. The PDF was extracted using the PDFGETN program[37] with Q_{max}=35 Å^{-1} and least-squares refinement of the PDF was performed using the PDFGUI frontend for PDFFIT2.[38] Crystal structures were visualized with ATOMEYE (Ref. 39) and VESTA.[40]

Reverse Monte Carlo simulations were run using RMCPROFILE version 6 (Ref. 41) on 7×7×7 cubic or 10×10×7 tetragonal spinel supercells with 19 208 or 19 600 atoms, respectively. A hard-sphere repulsion was applied to prevent M-O bond distances shorter than the first peak of the PDF but no clustering was observed at the cut-off distances. No preference for cation clustering was found, so configurations with randomized Cu and Mg occupancy were used. Simulations were performed as serial jobs on the HP Opteron QSR cluster at the California NanoSystems Institute.

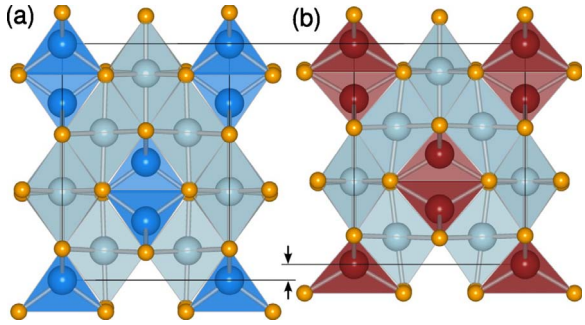

FIG. 2. (Color online) To scale, the pseudotetragonal cells of (a) cubic $MgCr_2O_4$ and (b) Jahn-Teller distorted tetragonal $CuCr_2O_4$ are viewed along the a axis of the $I4_1/amd$ cell. Contraction in the c direction is evident due to JT distortion in $CuCr_2O_4$. CrO_6 octahedra are light blue while MgO_4 and CuO_4 tetrahedra are dark blue and red, respectively.

Bond valence sums were extracted from atoms in the supercell in the same manner described in our previous work on $CuMn_2O_4$,[23] using the R_0 values of Brese and O'Keeffe.[42] CSM for AO_4 tetrahedra were calculated using a distance measure program provided by Pinsky and Avnir.

III. RESULTS AND DISCUSSION

A. Average structure via reciprocal-space analysis

The compounds $MgCr_2O_4$ and $CuCr_2O_4$ both belong to the AB_2O_4 spinel family of structures with the A cations, Mg^{2+} and Cu^{2+}, tetrahedrally coordinated by oxygen, while Cr^{3+} lies on the octahedral B site. The $[Ar]3d^3$ electron configuration of Cr^{3+} is very stable because each of the t_{2g} energy levels is singly occupied, so there is no tendency of site mixing or mixed valence.[43] Varying x in $Mg_{1-x}Cu_xCr_2O_4$ therefore does not disturb the B sublattice composition but changes in the interpenetrating A sublattice may lead to chemical pressure which will influence its size and shape.

On the tetrahedral A site, Mg^{2+} and Cu^{2+} have effectively identical ionic radii. Both are 0.57 Å as given by Shannon[44] but their electron configurations are distinctly different. Mg^{2+} has the [Ne] configuration and no d electrons. Cu^{2+} has $[Ar]3d^9$ and only two of the three t_2 energy levels are fully occupied in tetrahedral coordination (Fig. 1). This degeneracy causes a JT distortion, manifested by a flattening of the tetrahedron. Bond lengths are preserved but bond angles are no longer equivalent at 109.5°.[45–47] The contrasting behavior of Mg^{2+} and Cu^{2+} in tetrahedral coordination is evident when the $MgCr_2O_4$ and $CuCr_2O_4$ structures are compared in Fig. 2. $MgCr_2O_4$ forms in the cubic space group $Fd\bar{3}m$ with ideal MgO_4 tetrahedra.[48] $CuCr_2O_4$ undergoes flattening in the c direction and forms in the tetrahedral space group $I4_1/amd$,

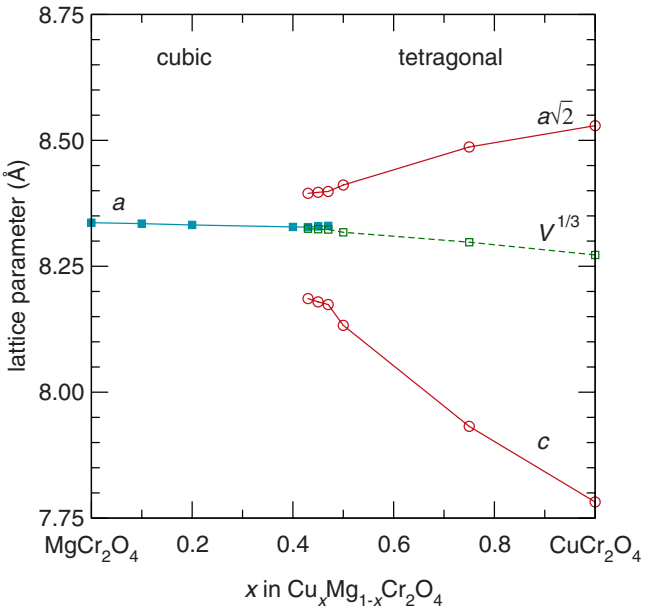

FIG. 3. (Color online) Lattice parameters of the $Mg_{1-x}Cu_xCr_2O_4$ solid solution obtained by Rietveld refinement of laboratory x-ray powder diffraction at room temperature. Coexistence of the cubic and tetragonal phases occurs for $0.43 \leq x \leq 0.47$. $V^{1/3}$ is shown for tetragonal phases. Error bars are smaller than the symbols for all points.

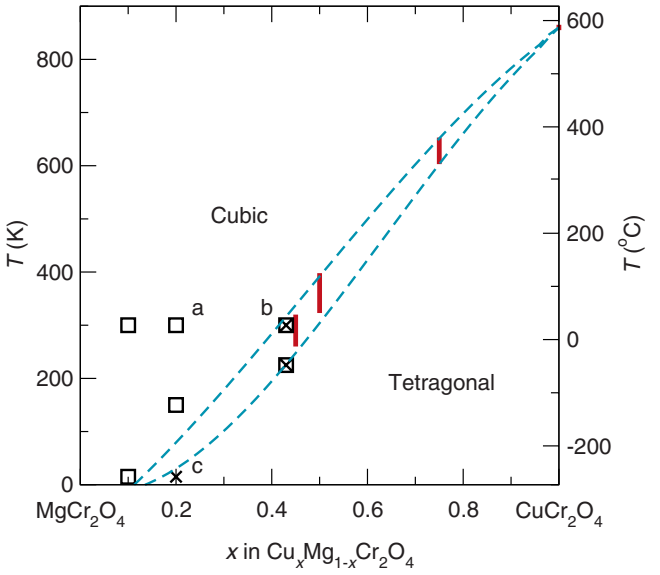

FIG. 4. (Color online) Phase diagram of the $Mg_{1-x}Cu_xCr_2O_4$ system as determined by Rietveld refinement. Points denote neutron refinements to cubic (□) and tetragonal (×) phases. Bars represent coexistence regions from high-temperature x-ray diffraction. Letters (a, b, c) correspond to the Rietveld refinements shown in Fig. 5.

which is the same space group as JT distorted Mn_3O_4 (and other AMn_2O_4) or $NiCr_2O_4$.[45,49] The unit cells are shown to scale in Fig. 2 to highlight their difference in dimensions.

Alloying x from 0 to 1 in $Mg_{1-x}Cu_xCr_2O_4$ produces a transition from a cubic to tetragonal spinel. The lattice parameters obtained from Rietveld refinements to room-temperature XRD patterns shown in Fig. 3 reveal that for $x<0.43$ a cubic spinel is formed with a gradually decreasing lattice parameter a. When $x=0.43$ the tetragonal phase appears with $c/a=0.975$ and a small region of coexistence persists for $0.43 \leq x \leq 0.47$, above which the cubic phase disappears. The compound becomes increasingly tetragonal as the end member $CuCr_2O_4$ is approached with $c/a=0.912$ when $x=1$. The pseudocubic cell volume contracts from 579.4 $Å^3$ for $MgCr_2O_4$ to 566.1 $Å^3$ for $CuCr_2O_4$, which is a 2.3% decrease.

We extend our Rietveld analysis using high-temperature XRD (HTXRD) and low-temperature TOF neutron scattering to produce an approximate phase diagram of the pseudobinary system $MgCr_2O_4$-$CuCr_2O_4$, shown in Fig. 4. The T_{JT} between cubic and tetragonal spinels has a nearly linear relationship on x. There is some phase coexistence determined from HTXRD denoted by the bars on the graph. We use the end-member $CuCr_2O_4$ transition of $T_{JT}=590$ °C from the literature.[49,50] The JT transition temperature steadily decreases with decreasing x so that the tetragonal phase occurs for $x=0.20$ but not for $x=0.10$ at $T=15$ K (the lowest temperature measured). Rietveld refinements to neutron-scattering data are shown in Fig. 5 for three different points on the phase diagram, representing (a) cubic, (b) mixed, and (c) tetragonal phases at $x=0.20$ and $T=300$ K, $x=0.43$ and $T=300$ K, and $x=0.20$ and $T=15$ K, respectively. In all cases, the fits are excellent. There is, however, some unfit intensity between split tetragonal peaks in (b) and (c), indicative of a more complex crystal structure than the two-phase Rietveld model would suggest.

Not shown on our phase diagram is the tetragonal distortion around 12 K in $MgCr_2O_4$.[51–53] A transition from $Fd\bar{3}m$ to $I4_1/amd$ occurs to remove the geometric frustration of

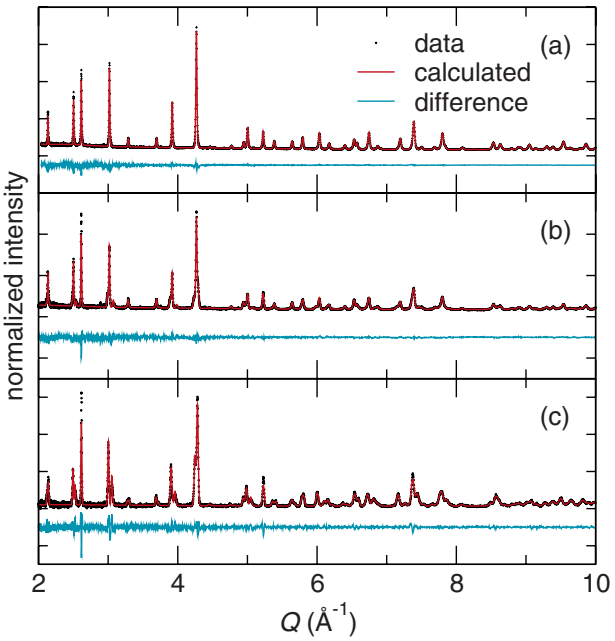

FIG. 5. (Color online) Time-of-flight neutron-scattering Rietveld refinements of $Mg_{1-x}Cu_xCr_2O_4$ with (a) $x=0.20$ at 300 K (cubic), (b) $x=0.43$ at 300 K (cubic and tetragonal), and (c) $x=0.20$ at 15 K (tetragonal).

Cr^{3+} spins arranged in a pyrochlore sublattice. Addition of magnetic Cu^{2+} cations in the A sites should relieve this frustration due to strong A-B interactions,[18,54] so we do not expect the spin-driven distortion to play a role for $x>0$. The sample with $x=0.10$ is cubic at 15 K.

The presence of a tetragonal phase for low Cu^{2+} content is surprising. At $x=0.20$, for instance, only one in five A sites has a JT active cation. The A cations are arranged in a diamond sublattice and each has four nearest A neighbors. The tetrahedra do not share edges or corners with each other, with the shortest exchange pathway being A-O-Cr-O-A. Given a random cation distribution, the probability of one Cu^{2+} having all JT-inactive Mg^{2+} neighbors is $(\frac{4}{5})^4=41.0\%$. The probability of having only one Cu^{2+} neighbor is $4(\frac{1}{5})(\frac{4}{5})^3=41.0\%$, and the probability of having two Cu^{2+} neighbors falls to $6(\frac{1}{5})^2(\frac{4}{5})^2=15.4\%$. Thus 82.0% of Cu^{2+} cations have zero or only one JT-active nearest neighbor but they still produce orbital ordering with long-range periodicity. The trend of T_{JT} versus x is roughly linear in Fig. 4 with no apparent jump at the percolation threshold of the diamond-type A sublattice.[55,56]

The critical concentration of Cu^{2+} needed to drive a cooperative JT distortion in $Mg_{1-x}Cu_xCr_2O_4$ at 300 K is $x=0.43$. This fraction increases with A-site cation radius in ACr_2O_4 spinels: $Zn_{1-x}Cu_xCr_2O_4$ ($r_{Zn}=0.60$ Å) is reported to have $x=0.47$ (Ref. 57) and $x=0.58$,[18] while $Cd_{1-x}Cu_xCr_2O_4$ ($r_{Cd}=0.78$ Å) has $x=0.64$.[20] This could be due to increased distance between A-site cations or a loosening of the structure (thus weakening of strain field produced by a JT distortion).

The critical concentration in $Zn_{1-x}Ni_xCr_2O_4$,[58] where Ni^{2+} drives JT distortion, is around $x\sim 1$ at room temperature. For Cr^{3+} on the spinel B site, less Cu^{2+} is needed to drive a cooperative distortion than Ni^{2+}. The $3d^8$ configuration of Ni^{2+} has only one unpaired t_2 electron, rather than the two of Cu^{2+}. The result is a smaller energy gain after breaking degeneracy and elongation (rather than contraction) of the c axis.[4]

Comparison with JT tendency of Mn^{3+} on the spinel B site is less direct. For example, the solid solution $Zn[Fe_{1-x}Mn_x]_2O_4$ has a critical concentration of about $x=0.3$,[59] while $Mn[Cr_{1-x}Mn_x]_2O_4$ has $x=0.4$.[60] This would seem to indicate a stronger JT tendency, in part due to closer B-B distances and edge sharing between octahedra. However, for $Zn_{x/2}Ge_{1-x/2}[Co_{1-x}Mn_x]_2O_4$, Wickham reports $x=0.65$,[61] and Bhandage reports $x=0.70$ for $Zn_{x/2}Mn_{1-x/2}[Ni_{1-x}Mn_x]_2O_4$.[62] The wide spread in critical concentrations of Mn^{3+} can be explained by the differences in JT splitting energies found by x-ray absorption spectroscopy on AMn_2O_4 spinels by Noh *et al.*[22] In essence, the energy drop from JT distortion around Mn^{3+} on the spinel B site is very sensitive to changes in chemical pressure.

We obtain the *cooperative* behavior of the averaged lattice using Rietveld refinement. We do not necessarily resolve the distinct cation coordination of Mg^{2+} and Cu^{2+} if they are different on the local, atomic length scale. Two views of the JT transition can be proposed: in the case of a sharp crossover, as would be implied by how Rietveld analysis is performed, all AO_4 tetrahedra are equivalent whether they contain Mg^{2+} or Cu^{2+}, and upon increasing x they abruptly transform from ideal tetrahedra in the cubic spinel to flattened tetrahedra in the cooperatively JT distorted spinel. In the second case, the CuO_4 tetrahedra are *always* locally JT distorted (even for values of x where the spinel is cubic) but the crossover at $x=0.43$ at room temperature represents the point where they cooperatively order and the JT distortions percolate through the long-range structure.

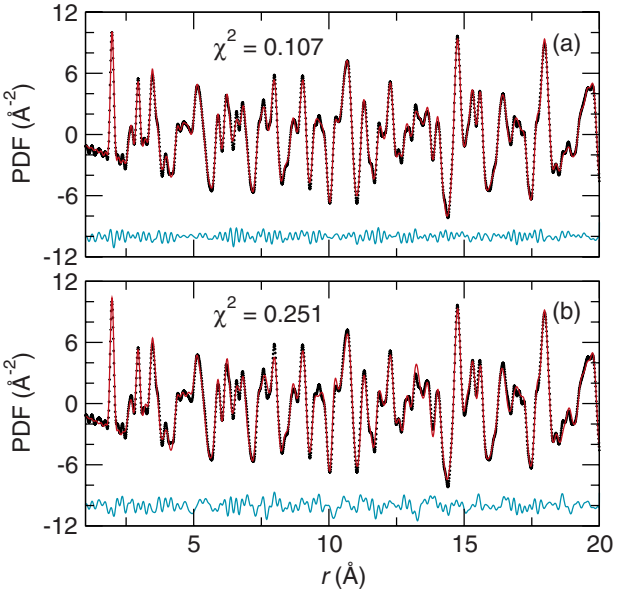

FIG. 6. (Color online) Least-squares fits to the PDF for $x=0.20$ at 300 K for the (a) cubic spinel phase with fractional occupancy obtained from Rietveld refinement and (b) an 80–20 fit to the end members $MgCr_2O_4$ and $CuCr_2O_4$.

B. Local structure via real-space analysis

The average structure model of $Mg_{1-x}Cu_xCr_2O_4$ from Rietveld refinement indicates that the compounds exist as single phases, either cubic or tetragonal, apart from the two-phase coexistence region around T_{JT}. When modeled using a single unit cell, Mg^{2+} and Cu^{2+} are required to share the same crystallographic site and their surroundings are necessarily identical. This model often inadequately describes the true structure of compounds where energy-lowering changes in cation coordination are known to persist above the average structural transition temperature as in perovskite manganites and cobaltites.[5,6,63,64] The PDF has emerged as a key tool for measuring these local distortions that do not possess long-range order. Because the PDF is a weighted histogram of all atom-atom distances in the sample, it is sensitive to the distinct bond distances that are produced by dissimilar coordination of multiple chemical species on the same site.[23] We investigate whether the PDF shows any signature of distinct Cu^{2+} and Mg^{2+} coordination.

Least-squares PDF refinements can be performed using the average structure unit cells from Rietveld refinement as a starting point. Fits to the $x=0.20$ data at 300 K are shown in Fig. 6. Panel (a) shows the fit to a Rietveld-refined cubic unit cell with split 0.20/0.80 occupancy of Cu^{2+} and Mg^{2+} on the same crystallographic site. In (b), we fit using a 0.20/0.80

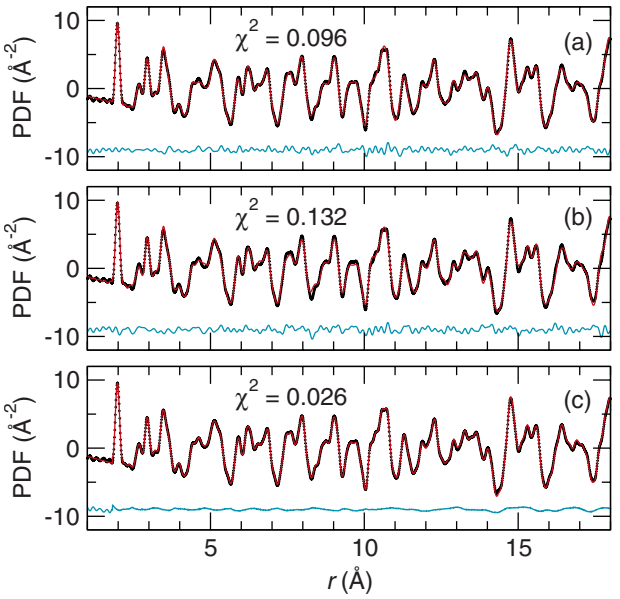

FIG. 7. (Color online) Fits to the PDF for $x=0.43$ at 300 K for (a) least-squares refinement of the two fractional-occupancy phases found from Rietveld refinement, (b) least-squares refinement using the end members $MgCr_2O_4$ and $CuCr_2O_4$, and (c) the fit after RMC simulation.

linear combination of the $MgCr_2O_4$ and $CuCr_2O_4$ end members with lattice parameters allowed to refine. The fit is good despite the use of a tetragonal unit cell to model a structure far above T_{JT} but it does not improve on the fit using a single cubic unit cell. We use the value

$$\chi^2 = \sum \frac{(\mathrm{PDF}^{obs} - \mathrm{PDF}^{calc})^2}{N} \quad (1)$$

to compare fits, where N is the number of points in the PDF from the nearest-neighbor cutoff to 20 Å. The ability to distinguish Mg and Cu is hindered by their similar neutron-scattering lengths: 5.38 fm and 7.71 fm, respectively.[65] For $x=0.20$, least-squares PDF fits do not definitively prove that there are distinct (or identical) coordination environments for Mg^{2+} and Cu^{2+}.

Resolution of distinct cation environments is aided when $x=0.43$ due to approximately even concentrations of Cu^{2+} and Mg^{2+}. At 300 K, Rietveld refinement found coexistence of the cubic and tetragonal phases. Neither phase alone can be used to produce a satisfactory fit to the PDF. A two-phase fit using the Rietveld refined cells is shown in Fig. 7(a) and agrees quite well with the data. As with the $x=0.20$ sample, we also fit the data to a combination of the end members $MgCr_2O_4$ and $CuCr_2O_4$ in Fig. 7(b). Again, the fractional occupancy Rietveld result produces a better fit than the end members. The least-squares fits indicate that the average structures produce excellent representations of the local structures but they do not definitively show whether the Mg^{2+} and Cu^{2+} coordination environments are distinct or similar.

Least-squares fits to the PDF are required to specify how many distinct AO_4 environments to allow, much like in a Rietveld refinement. The $Fd\bar{3}m$ and $I4_1/amd$ unit cells provide only one AO_4 environment per phase. There is no way to define cation-dependent coordination without manually building a lower-symmetry unit cell. In order to investigate the AO_4 environment directly, we remove the symmetry constraints of least-squares PDF analysis and utilize large-box modeling via RMC simulations. This method has proved to be useful for investigating atomic structure on the local level, especially in cases where long-range periodicity is not present, such as $SrSnO_3$,[28] $Bi_2Ti_2O_7$,[34] and β-cristobalite.[66]

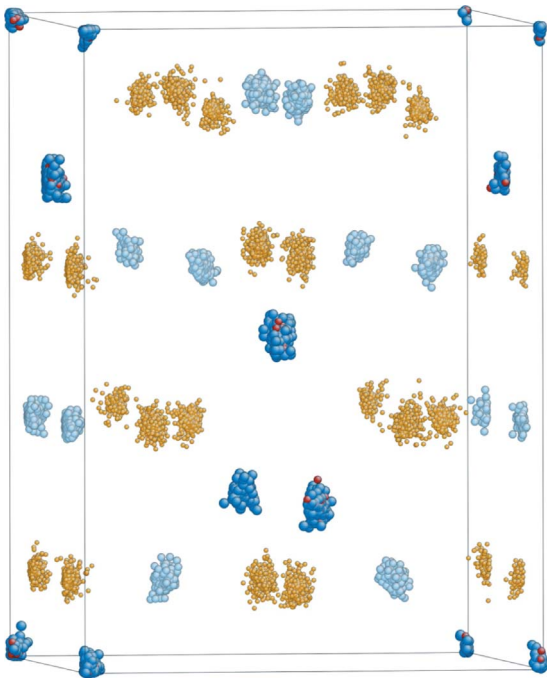

FIG. 8. (Color online) The final $10\times10\times7$ RMC supercell for an $x=0.20$ simulation is folded into a single unit cell to obtain point clouds at each crystallographic site. Atoms shown are Cu (red), Mg (dark blue), Cr (light blue), and O (orange).

The RMC supercell for an $x=0.20$ sample at 15 K is inspected by folding each of the unit cells back into a single box, shown in Fig. 8, which reveals how each crystallographic site is decorated with atoms. The supercell contains 560 Cu and 2240 Mg atoms that are randomly arranged. Because there are a large number of distinct Cu and Mg atoms, statistical analysis can be used to investigate whether there is any evidence for the local AO_4 distortion to depend on the central cation. Bond valence sum histograms shown in Fig. 9 show that both the A cations have valences peaked around the expected value of A^{2+}, and the B site shows only Cr^{3+}, which implies that our supercells contain chemically reasonable bond lengths.

No cation dependence of AO_4 bond distances is obvious from partial radial distributions $g_{Cu\text{-}O}(r)$ and $g_{Mg\text{-}O}(r)$. This is to be expected because Mg^{2+} and Cu^{2+} have the same ionic radius when tetrahedrally coordinated. Neither is there any apparent distinction between CuO_4 and MgO_4 tetrahedra based upon O-A-O bond angles, in contrast to our previous study on $CuMn_2O_4$.[23]

We use the CSM technique to gauge the tendency for JT distortion of AO_4 tetrahedra. The CSM technique provides a

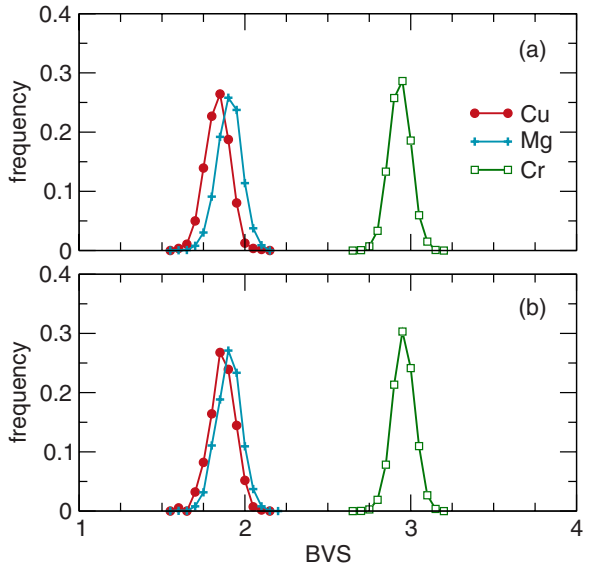

FIG. 9. (Color online) Bond valence sums for Cu and Mg extracted from $Mg_{1-x}Cu_xCr_2O_4$ RMC supercells $x=0.20$ after fits to data at (a) $T=300$ K and (b) 15 K. Aside from a slight broadening at 300 K, the distributions are comparable.

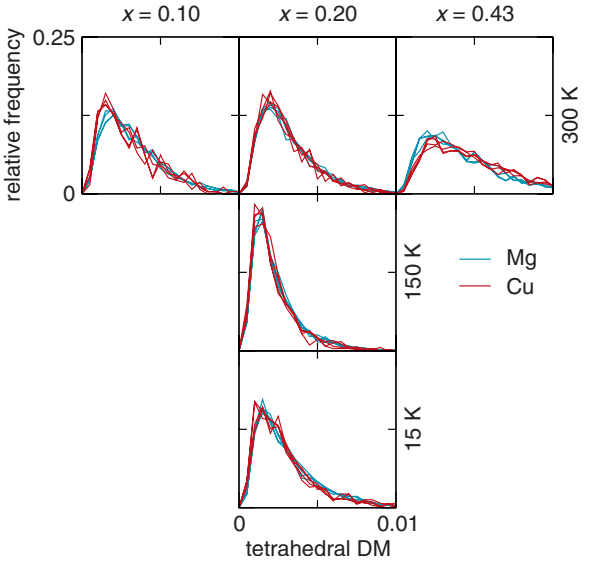

FIG. 10. (Color online) CSM histograms from RMC simulations for three Cu contents and three temperatures. Each panel contains eight distributions: one Cu and one Mg for four independent simulations. Broadening across the $T=300$ K series indicates increasing tetrahedral distortion with x. Thermal effects lead to sharpening and shifting toward smaller DM when the $x=0.20$ sample is cooled to 150 K. This tendency toward ideal tetrahedra is disrupted by long-range tetragonal distortion upon further cooling, so the $T=15$ K histogram is broad and shifted to higher DM.

distance measure (DM) of a given tetrahedron that indicates its deviation from ideality.[30,31] A perfect tetrahedron has DM=0 and any distortion increases the value of DM. In the end member compounds, MgO_4 has a DM=0 while CuO_4 has a DM=0.0076. Having thousands of distinct tetrahedra in the RMC supercell affords the opportunity to produce a histogram of DM (Fig. 10) for all tetrahedra depending on the central cation. Each panel contains eight lines: four for each cation, resulting from four independent RMC simulations. The overall shape of each histogram describes the average distortion (peak center) and the tightness of the DM distribution (peak width) at each value of x and T. No tetrahedra are present with exactly DM=0 because stochastic RMC simulations leave no atomic positions untouched, even a compound with ideal tetrahedra would have the shapes subtly distorted.

At 300 K, the spread of distortions increases for $x=0.43$ because the average structure becomes a mixture of cubic and tetragonal phases. In the series where $x=0.20$, the peak sharpens upon cooling to 150 K, which we attribute to a reduction in thermal vibrations. It also moves to smaller DM values, indicating a tendency toward a more ideal MO_4 environment. This trend would continue to low temperature in the absence of long-range JT distortion. Instead, the peak broadens and shifts to higher DM at 15 K. We attribute both of these effects to the tetragonal phase transition. These histograms provide a view of the average tetrahedral shape but no distinction between Mg and Cu is apparent. We find that cumulative distributions offer a clearer picture of this dependence.

The cumulative distributions in Fig. 11 do not show separation between the Cu and Mg curves in the $x=0.10$ or 0.20 samples. However, the $x=0.43$ sample shows a clear distinction with Mg tetrahedra possessing DM that are closer to zero (more ideal) than Cu. This is clear evidence for the tendency of Cu to undergo JT distortion while Mg remains more symmetric.

Overlapping DM curves for $x=0.10$ and 0.20 do not preclude the possibility of distinct CuO_4 and MgO_4 tetrahedra in those samples. There may be insufficient resolution in the PDF to distinguish the cations due to their similar neutron-

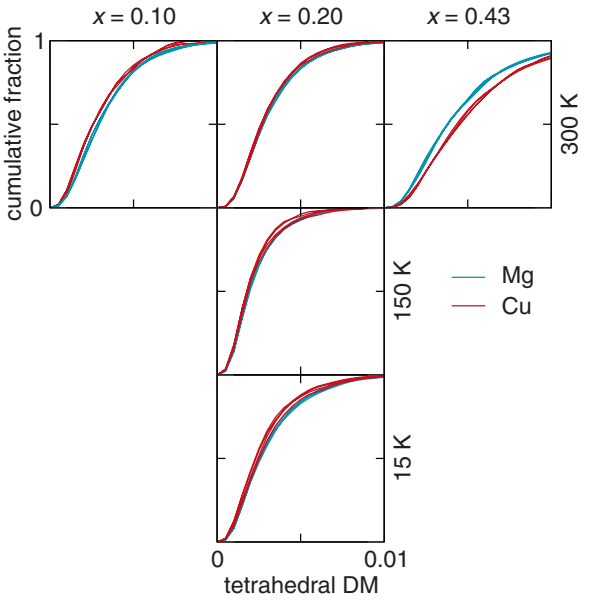

FIG. 11. (Color online) Cumulative CSM distributions are similar enough from run to run that most lines overlay each other. Only the $x=0.43$ run has a clear distinction between CuO_4 and MgO_4 tetrahedron shape with MgO_4 distinctly more ideal than CuO_4.

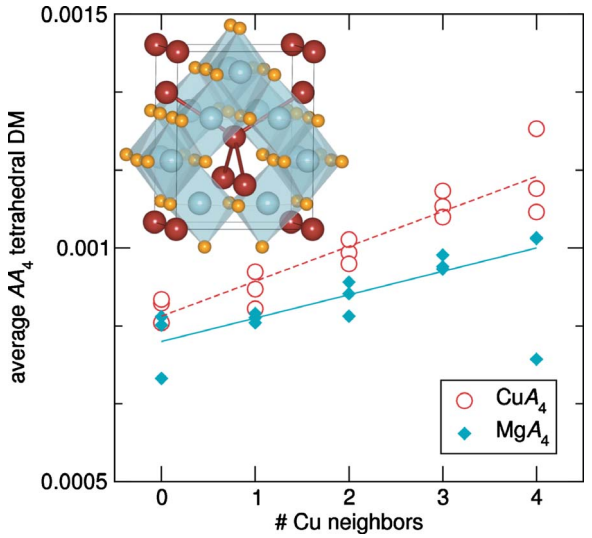

FIG. 12. (Color online) CSM distributions of AA_4 tetrahedra (connected by long red bonds in inset) as a function of number of neighbors that are JT-active Cu^{2+}. Distinct distributions are shown for CuA_4 (circles) and MgA_4 (diamonds). Linear guide to the eyes for each distribution show increasing tetrahedral distortion with number of Cu neighbors and overall more distorted tetrahedra when tetrahedra are Cu centered.

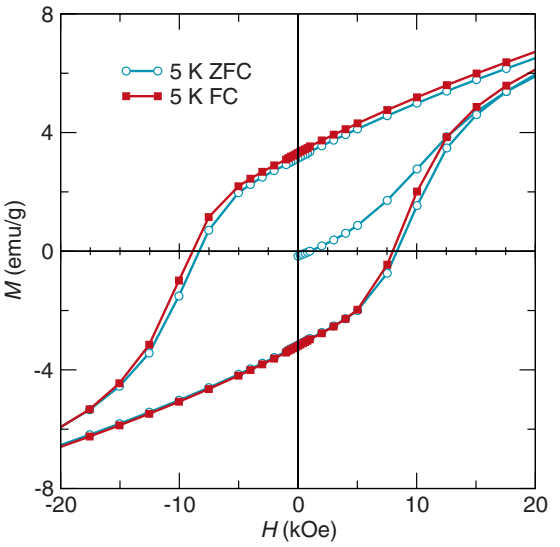

FIG. 13. (Color online) Magnetic hysteresis of $Mg_{1-x}Cu_xCr_2O_4$ with $x=0.43$ at $T=5$ K after zero-field cooling (ZFC) and FC with $H_{FC}=5$ T. The shift in the $-H$ direction when $M=0$ is the exchange bias field H_E.

scattering cross sections and the relatively low concentration of Cu^{2+}. It remains unclear whether distinct cation environments are only seen around $x=0.5$ (due to approximately even cation concentrations) and if the distinction would disappear as $x \rightarrow 1$. Temperature dependence of the CSM when $x=0.43$ may also provide some insight into the dynamics of these distortions. Substituting a JT-inactive A-site cation with a different neutron-scattering cross length, such as Mn^{2+} or Co^{2+}, may aid contrast with Cu^{2+}.

Short-range interactions between JT-active cations are evident in the A-A correlations in Fig. 12. Each A cation has four A nearest neighbors 3.59 Å away, arranged in a diamond lattice (inset in Fig. 12). The four nearest neighbors create a large tetrahedron around the central cation. The tetrahedral DM for these AA_4 are plotted for each central cation (Mg or Cu) as a function of the number of Cu nearest neighbors, from 0 to 4. Multiple RMC simulations show an upward trend indicating more distortion as the number of nearby Cu increases. The separation between the two lines implies that Cu-centered CuA_4 have higher tetrahedral DM (more distortion) than Mg-centered MgA_4. These short-range correlations are indicative of strain coupling between adjacent A-site JT distortions.

C. Magnetic properties

$MgCr_2O_4$ and $CuCr_2O_4$ have markedly different magnetic behavior due to the addition of unpaired spins in Cu^{2+} and the accompanying JT distortion. $CuCr_2O_4$ is a hard ferrimagnet with $T_C=135$ K,[67] while $MgCr_2O_4$ undergoes complex antiferromagnetic (AFM) ordering below $T_N=16$ K.[53,68] Macroscopic composites of a ferromagnet (FM) and antiferromagnet would result in a traditional exchange biased material, with an enhanced coercive field H_C and an exchange bias field H_E, manifested as a shift of the hysteresis loop in the $-H$ direction.[69–71]

The $Mg_{1-x}Cu_xCr_2O_4$ solid solution is a mixture on the atomic level but nevertheless exhibits the magnetic hallmarks of an exchange biased system. The hysteresis loop of the $x=0.43$ sample in Fig. 13 at $T=5$ K has $H_C=8.4$ kOe. Cooling with a field $H_{FC}=50$ kOe broadens the hysteresis loop and shifts it in the $-H$ direction by $H_E=0.44$ kOe. This shift signifies the preference for the ferrimagnet to align along the field-cooling (FC) direction. H_C and H_E decrease with the Cu^{2+} concentration x, as does the onset of magnetic ordering. These trends are shown in Fig. 14. In all cases, field-cooling increases H_C and results in the appearance of a significant H_E. We find $H_E=0$ in all samples after zero FC (ZFC).

Exchange bias is traditionally manifested by pinning at the interface between a ferromagnet or ferrimagnet and antiferromagnet after field cooling when $T_C > T_N$. It can also arise from intrinsic disorder in a single-phase system or the presence of disordered spins from either a spin glass or uncompensated surface spins on small particles (which behave in a glassy manner themselves).[72,73] In the $Mg_{1-x}Cu_xCr_2O_4$ system, the magnetic behavior cannot be fully described by traditional AFM-FM interplay between $MgCr_2O_4$ and $CuCr_2O_4$ because the onset of H_E when $x=0.43$ in Fig. 14 occurs above $T=20$ K, which is above the Néel temperature of $MgCr_2O_4$. Therefore the disordered solid solution contains some regions of heterogeneity which may behave as glassy moments or as some intermediate AFM phase. Either of these cases can produce exchange bias.[18,74]

The correlations between A cations seen in Fig. 12 indicate that the local structure varies with the composition of nearby atoms. Magnetic interactions, in turn, will be affected by these local distortions. A more detailed investigation of magnetic behavior, as was performed on $Zn_xMn_{3-x}O_4$,[55] may

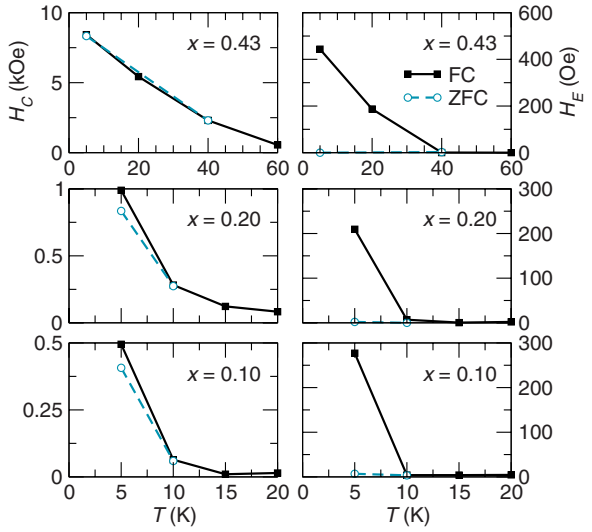

FIG. 14. (Color online) Coercive fields H_C (left) and exchange bias fields H_E (right) for $Mg_{1-x}Cu_xCr_2O_4$ samples with $x=0.43$, 0.20, and 0.10 after ZFC and FC with $H_{FC}=5$ T. In all cases, ZFC results in a smaller H_C and gives $H_E=0$.

help elucidate how the competing structural and magnetic interactions produce exchange bias. The phenomenon of JT-active cation clustering has been investigated by dilatometry[75] but its effects on magnetism have not been explored in detail.

IV. CONCLUSIONS

We find that the solid solution $Mg_{1-x}Cu_xCr_2O_4$ has a two-phase coexistence of cubic and tetragonal phases at room temperature for $0.43 \leq x \leq 0.47$. Tetragonality is induced by increasing JT activity in tetrahedrally coordinated Cu^{2+}. The average structure descriptions from Rietveld refinement provide an adequate description of the structures across the range of x and temperature. This is corroborated by the magnetic behavior, which indicates a disordered atomic mixture. The $x=0.20$ sample is cooperatively JT distorted with orbital ordering at 15 K despite 82% of all Cu^{2+} having zero or only one Cu^{2+} neighbors.

Least-squares PDF refinements achieve good fits using the models from Rietveld refinement, implying that it might be difficult to improve on models where CuO_4 and MgO_4 are equivalent. Still, bond valence calculations show that RMC simulations produce better fits to the data while retaining chemically reasonable bond distances. The AO_4 tetrahedral distortion increases with x as judged by CSM. The absence of distinct CuO_4 local distortions in the low-x CSM histograms does not prohibit their existence. When $x=0.43$, tetrahedral DM indicates distinct coordination of Cu^{2+} versus Mg^{2+}. Furthermore, cation-cation interactions probed by AA_4 CSM indicate that local clustering of Cu leads to increased JT distortion. This technique resolves cation-dependent JT distortions (even when they are incoherent) in materials where contrast between cations exists. The presence of magnetic exchange bias implies that short-range structural details are influencing the magnetic interactions and more complex magnetic characterization may help describe these interactions.

ACKNOWLEDGMENTS

We thank Maosheng Miao, Katharine Page, Graham King, Anna Llobet, and Thomas Proffen for helpful discussions. This work has benefited from the use of NPDF at the Lujan Center at Los Alamos Neutron Science Center, funded by DOE Office of Basic Energy Sciences. Los Alamos National Laboratory is operated by Los Alamos National Security LLC under DOE under Contract No. DE-AC52-06NA25396. This work was supported by the Institute for Multiscale Materials Studies and the National Science Foundation (Grant No. DMR 0449354). The MRL Central Facilities are supported by the MRSEC Program of the NSF (Grant No. DMR 05-20415); a member of the NSF-funded Materials Research Facilities Network (www.mrfn.org).

*dshoe@mrl.ucsb.edu
†seshadri@mrl.ucsb.edu

[1] J. G. Bednorz and K. A. Müller, Z. Phys. B: Condens. Matter **64**, 189 (1986).
[2] E. Pavarini, I. Dasgupta, T. Saha-Dasgupta, O. Jepsen, and O. K. Andersen, Phys. Rev. Lett. **87**, 047003 (2001).
[3] H. A. Jahn and E. Teller, Proc. R. Soc. London, Ser. A **161**, 220 (1937).
[4] M. Gerloch, Inorg. Chem. **20**, 638 (1981).
[5] X. Qiu, T. Proffen, J. Mitchell, and S. Billinge, Phys. Rev. Lett. **94**, 177203 (2005).
[6] A. Sartbaeva, S. A. Wells, M. F. Thorpe, E. S. Bozin, and S. J. L. Billinge, Phys. Rev. Lett. **99**, 155503 (2007).
[7] E. Dagotto, *Nanoscale Phase Separation and Colossal Magnetoresistance: The Physics of Manganites and Related Compounds* (Springer, New York, 2003).
[8] P. J. Wojtowicz, Phys. Rev. **116**, 32 (1959).
[9] R. Englman and B. Halperin, Phys. Rev. B **2**, 75 (1970).
[10] M. Uehara, S. Mori, C. H. Chen, and S. Cheong, Nature (London) **399**, 560 (1999).
[11] S. Yeo, Y. Horibe, S. Mori, C. M. Tseng, C. H. Chen, A. G. Khachaturyan, C. L. Zhang, and S. Cheong, Appl. Phys. Lett. **89**, 233120 (2006).
[12] C. L. Zhang, S. Yeo, Y. Horibe, Y. J. Choi, S. Guha, M. Croft, S. Cheong, and S. Mori, Appl. Phys. Lett. **90**, 133123 (2007).
[13] S. Park *et al.*, Nano Lett. **8**, 720 (2008).
[14] C. Leroux, A. Loiseau, D. Broddin, and G. Vantendeloo, Philos. Mag. B **64**, 57 (1991).
[15] Y. Le Bouar, A. Loiseau, and A. G. Khachaturyan, Acta Mater. **46**, 2777 (1998).
[16] P. Fratzl, O. Penrose, and J. L. Lebowitz, J. Stat. Phys. **95**, 1429 (1999).

[17] J. L. MacManus-Driscoll, Adv. Funct. Mater. **20**, 2035 (2010).
[18] L.-Q. Yan, F. Maciá, Z.-W. Jiang, J. Shen, L.-H. He, and F.-W. Wang, J. Phys.: Condens. Matter **20**, 255203 (2008).
[19] Y. Kino and S. Miyahara, J. Phys. Soc. Jpn. **21**, 2732 (1966).
[20] L. Q. Yan, Z. W. Jiang, X. D. Peng, L. H. He, and F. W. Wang, Powder Diffr. **22**, 340 (2007).
[21] S. Waplak and W. Bednarski, J. Phys.: Condens. Matter **14**, 12529 (2002).
[22] H. Noh, S. Yeo, J. Kang, C. L. Zhang, S. Cheong, S. Oh, and P. D. Johnson, Appl. Phys. Lett. **88**, 081911 (2006).
[23] D. P. Shoemaker, J. Li, and R. Seshadri, J. Am. Chem. Soc. **131**, 11450 (2009).
[24] R. L. McGreevy, Nucl. Instrum. Methods Phys. Res. A **354**, 1 (1995).
[25] R. L. McGreevy, J. Phys.: Condens. Matter **13**, R877 (2001).
[26] S. T. Norberg, I. Ahmed, S. Hull, D. Marrocchelli, and P. A. Madden, J. Phys.: Condens. Matter **21**, 215401 (2009).
[27] O. Cambon, J. Haines, M. Cambon, D. A. Keen, M. G. Tucker, L. Chapon, N. K. Hansen, M. Souhassou, and F. Porcher, Chem. Mater. **21**, 237 (2009).
[28] A. L. Goodwin, S. A. T. Redfern, M. T. Dove, D. A. Keen, and M. G. Tucker, Phys. Rev. B **76**, 174114 (2007).
[29] S. Wells, M. T. Dove, and M. G. Tucker, J. Appl. Crystallogr. **37**, 536 (2004).
[30] H. Zabrodsky, S. Peleg, and D. Avnir, J. Am. Chem. Soc. **114**, 7843 (1992).
[31] M. Pinsky and D. Avnir, Inorg. Chem. **37**, 5575 (1998).
[32] S. Keinan and D. Avnir, J. Chem. Soc. Dalton Trans. **2001**, 941.
[33] K. M. Ok, P. S. Halasyamani, D. Casanova, M. Llunell, P. Alemany, and S. Alvarez, Chem. Mater. **18**, 3176 (2006).
[34] D. P. Shoemaker, R. Seshadri, A. L. Hector, A. Llobet, T. Proffen, and C. J. Fennie, Phys. Rev. B **81**, 144113 (2010).
[35] J.-F. Bérar and G. Baldinozzi, IUCR Newsl. **20**, 3 (1998).
[36] A. Larson and R. Von Dreele, Los Alamos National Laboratory Report No. LAUR 86-748, 2000 (unpublished).
[37] P. F. Peterson, M. Gutmann, T. Proffen, and S. J. L. Billinge, J. Appl. Crystallogr. **33**, 1192 (2000).
[38] C. L. Farrow, P. Juhas, J. W. Liu, D. Bryndin, E. S. Bozin, J. Bloch, T. Proffen, and S. J. L. Billinge, J. Phys.: Condens. Matter **19**, 335219 (2007).
[39] J. Li, Modell. Simul. Mater. Sci. Eng. **11**, 173 (2003).
[40] K. Momma and F. Izumi, J. Appl. Crystallogr. **41**, 653 (2008).
[41] M. G. Tucker, D. A. Keen, M. T. Dove, A. L. Goodwin, and Q. Hui, J. Phys.: Condens. Matter **19**, 335218 (2007).
[42] N. E. Brese and M. O'Keeffe, Acta Crystallogr., Sect. B: Struct. Sci. **47**, 192 (1991).
[43] A. Miller, J. Appl. Phys. **30**, S24 (1959).
[44] R. D. Shannon, Acta Crystallogr., Sect. A: Cryst. Phys., Diffr., Theor. Gen. Crystallogr. **32**, 751 (1976).
[45] W. A. Dollase and H. S. C. O'Neill, Acta Crystallogr., Sect. C: Cryst. Struct. Commun. **53**, 657 (1997).
[46] N. N. Greenwood and A. Earnshaw, *Chemistry of the Elements*, 2nd ed. (Butterworth-Heinemann, London, 1997).
[47] M. C. Day and J. Selbin, *Theoretical Inorganic Chemistry* (Reinhold, New York, 1962).
[48] E. J. W. Verwey and E. L. Heilmann, J. Chem. Phys. **15**, 174 (1947).
[49] B. J. Kennedy and Q. Zhou, J. Solid State Chem. **181**, 2227 (2008).
[50] M. Tovar, R. Torabi, C. Welker, and F. Fleischer, Physica B **385-386**, 196 (2006).
[51] H. Ehrenberg, M. Knapp, C. Baehtz, and S. Klemme, Powder Diffr. **17**, 230 (2002).
[52] S. Klemme and M. Ahrens, Phys. Chem. Miner. **34**, 59 (2007).
[53] L. Ortega-San-Martín, A. J. Williams, C. D. Gordon, S. Klemme, and J. P. Attfield, J. Phys.: Condens. Matter **20**, 104238 (2008).
[54] Z. Zhang, D. Louca, A. Visinoiu, S. Lee, J. Thompson, T. Proffen, A. Llobet, Y. Qiu, S. Park, and Y. Ueda, Phys. Rev. B **74**, 014108 (2006).
[55] D. P. Shoemaker, E. E. Rodriguez, R. Seshadri, I. S. Abumohor, and T. Proffen, Phys. Rev. B **80**, 144422 (2009).
[56] S. C. van der Marck, Phys. Rev. E **55**, 1514 (1997).
[57] D. Reinen, M. Atanasov, G. Nikolov, and F. Steffens, Inorg. Chem. **27**, 1678 (1988).
[58] Y. Kino, B. Lüthi, and M. E. Mullen, J. Phys. Soc. Jpn. **33**, 687 (1972).
[59] M. O'Keeffe, J. Phys. Chem. Solids **21**, 172 (1961).
[60] P. Holba, M. Nevriva, and E. Pollert, Mater. Res. Bull. **10**, 853 (1975).
[61] D. G. Wickham and W. J. Croft, J. Phys. Chem. Solids **7**, 351 (1958).
[62] G. T. Bhandage and H. V. Keer, J. Phys. C **11**, L219 (1978).
[63] E. S. Božin, M. Schmidt, A. J. DeConinck, G. Paglia, J. F. Mitchell, T. Chatterji, P. G. Radaelli, T. Proffen, and S. J. L. Billinge, Phys. Rev. Lett. **98**, 137203 (2007).
[64] D. Louca and J. Sarrao, Phys. Rev. Lett. **91**, 155501 (2003).
[65] V. F. Sears, Neutron News **3**, 26 (1992).
[66] M. G. Tucker, M. P. Squires, M. T. Dove, and D. A. Keen, J. Phys.: Condens. Matter **13**, 403 (2001).
[67] H. Walter, I. Schulz, and J. Scheve, Z. Anorg. Allg. Chem. **352**, 241 (1967).
[68] H. Shaked, J. M. Hastings, and L. M. Corliss, Phys. Rev. B **1**, 3116 (1970).
[69] W. H. Meiklejohn and C. P. Bean, Phys. Rev. **102**, 1413 (1956).
[70] A. E. Berkowitz and K. Takano, J. Magn. Magn. Mater. **200**, 552 (1999).
[71] J. Nogués, J. Sort, V. Langlais, V. Skumryev, S. Suriñach, J. S. Muñoz, and M. D. Baró, Phys. Rep. **422**, 65 (2005).
[72] S. A. Makhlouf, F. T. Parker, and A. E. Berkowitz, Phys. Rev. B **55**, R14717 (1997).
[73] B. Martínez, X. Obradors, L. Balcells, A. Rouanet, and C. Monty, Phys. Rev. Lett. **80**, 181 (1998).
[74] M. Ali, P. Adie, C. H. Marrows, D. Greig, B. J. Hickey, and R. L. Stamps, Nature Mater. **6**, 70 (2007).
[75] V. A. M. Brabers, J. Phys. Chem. Solids **32**, 2181 (1971).